PROCEEDINGS of the
23rd International Congress on Acoustics

9 to 13 September 2019 in Aachen, Germany

AN EXPERIMENTAL STUDY ON AEROACOUSTICS AND SHOCK DYNAMICS ASSOCIATED WITH HARTMANN WHISTLE

Sonu THOMAS[1]; K SRINIVASAN[2]

[1] Indian Institute of Technology Madras, India

[2] Indian Institute of Technology Madras, India

ABSTRACT

Experiments are conducted to study the mechanisms involved in the workings of a cylindrical Hartmann whistle at two different NPRs. The focus is more on the shock dynamics associated with the Hartmann whistle phenomenon. The sound field of the order of 130 dB is produced. Distinct peaks are observed at the fundamental frequency as well as the higher harmonics. The relationship between the flow pattern seen form Schlieren data with the acoustic measurements is highlighted. The cavity gas oscillation and the high speed Schlieren data showed the non-sinusoidal movement pattern of the stand-off shock. The static pressure variation in an under-expanded jet is found to be responsible for non-sinusoidal shock movement.

Keywords: Hartmann whistle, Shock-dynamics, resonance

1 INTRODUCTION

Hartmann whistles have been a subject of investigation for almost a century now. Hartmann whistle consists of a sonic under-expanded jet impinging on the open end of a cavity, placed in line with the axis of the jet. When the open end of the cavity is kept at certain regions of the under-expanded jet, strong flow oscillations occur. The regions where these strong oscillations occur are termed as regions of instability, which was explained by Smith and Powell (1,2). These devices are used to produce strong unsteady flow fields and high temperature at closed end. Since these devices employ no-moving-part, it is more reliable and safe to operate. These devices are also capable of producing resonance induced heating attending around 1000 K, which can be used for heating related applications. In few literatures, this device is also referred to as the Powered Resonance Tube (PRT) (3–5), as the power source is the constant high pressure air supply. Sarohia and Back (6) identified the different operational modes of Hartmann whistle; namely, jet instability mode, jet regurgitant mode, and jet screech mode. In the case of an under-expanded jet, the 'jet regurgitant mode' is usually in operation. The strong oscillations thus caused produces high intensity acoustic radiation of discrete nature. These devices can be tuned to any desired frequency. The resonance frequencies are strong function of the geometry of the Hartmann whistle, especially the length of the tube. Raman and co-workers (3,5,7) have used resonant acoustics produced by Hartmann whistle in Active Flow Control (AFC) applications. Raman and Srinivasan (4) gave a comprehensive review that includes plethora of work done over a period of 90 years. Sreejith *et al.* (8) studied the aero-acoustic aspects of a conical Hartmann resonator and compared the results with a conventional cylindrical Hartmann whistle. Recently, Narayanan *et al.* (9–13) conducted comprehensive studies to understand the influence of geometrical aspects affecting the aero-acoustic behavior (such as spectra and directivity) of the resonator. Narayanan *et al.* (14) also used the intense acoustic field produced by Hartmann whistle to enhance the fuel droplet atomization. More recently, Lu and Liu (15) used forward facing cavity (shaped like a Hartmann resonator) as part of the thermal protection mechanism in a hyper-sonic vehicle, to reduce heating. Huang *et al.* (16) showed that by using a forward facing cavity embedded in the fore-body of a hypersonic vehicle, drag and stagnation point heat flux can be reduced. XinDong *et al.* (17) showed that the forward facing nose cavity can act as a thermal protection for a hypersonic vehicle.

[1] sonuthomas9100@gmail.com
[2] ksri@iitm.ac.in

Form the literature it is clear that, given that these find its use in many practical applications. Hence, it is important to understand the underlying mechanisms involved Hartmann whistle operation. This understanding can used to tailor this device for a specific application. The intended work primarily focuses on the study of the mechanisms involved in the Hartmann whistle working. In the present study aspects like, acoustic data (spectrum and directivity), cavity gas oscillation and high speed Schlieren flow visualization for a cylindrical Hartmann whistle are compared at two different Nozzle Pressure Ratios (NPRs). The main intend of the present work is to understand the underlying physics of such flows interacting with open-closed end cavity in detail. A detailed study of these aspects can give a better physical understanding of the device Hartmann cavity performance.

2 EXPERIMENTAL SETUP

2.1 Anechoic test facility and other arrangement

All the experiments are conducted in an anechoic test facility (see Figure 1). The anechoic chamber has dimensions of 2.5 m x 2 m x 2 m (wedge tip-to-tip). The cut-off frequency of chamber is 700 Hz. High compressed air is delivered to the settling chamber at a pressure of 9 bar. The upstream of the settling chamber is fitted with a moisture remover, an air filter, and a pressure regulator. The air filter removes particles above 5-microns in size. The stagnation pressure inside the settling chamber is controlled using pressure regulator valve. Flow conditioning meshes of progressive fineness are provided in the settling chamber to reduce the initial turbulence level.

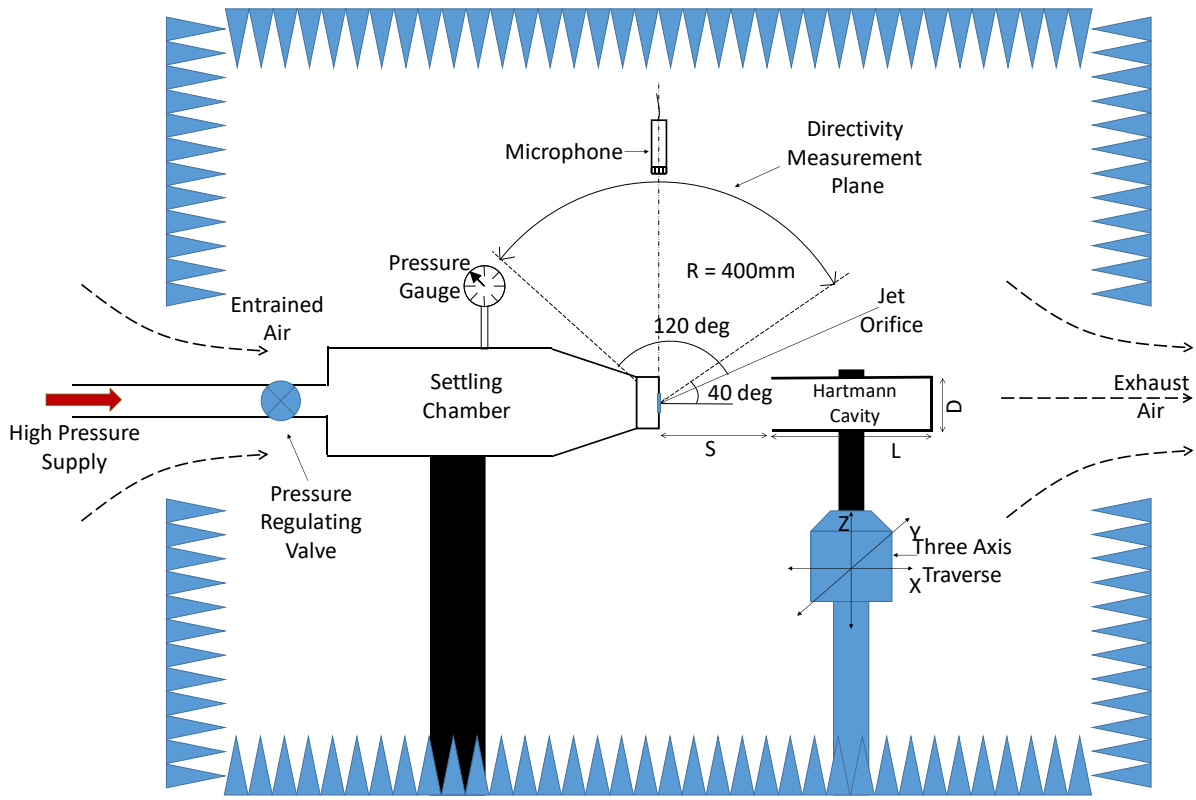

Figure 1 – Schematic of the anechoic test facility and experimental setup

The experimental setup (see Figure 1) also consists of an under-expanded jet issuing from a 10 mm orifice diameter, impinging on Hartmann cavity. Provision is made to connect a dynamic pressure sensor at the closed end of Hartmann cavity. The entire Hartmann test setup is bracketed on a compound rest, which had movement control in all three axes direction. Angular traverse mounted with a microphone is used to measure the directivity of the sound field at different emission angles. The angle is varied from 40° to 120° in steps of 5°. The 0° coincides with jet axis direction. Figure 2 shows the picture of the setup kept in the anechoic facility.

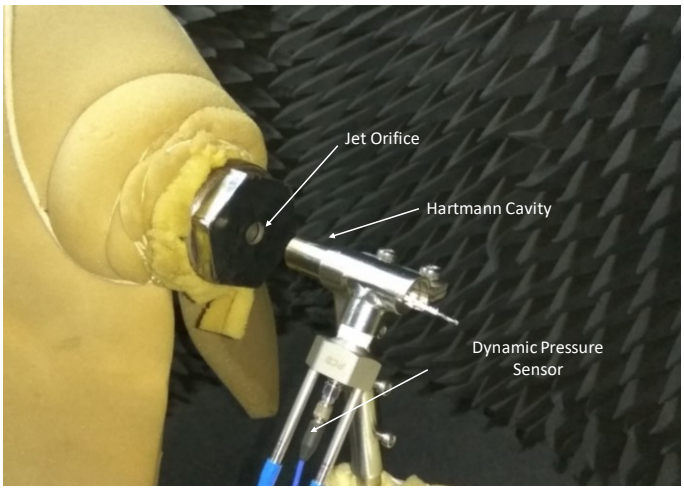

Figure 2 – Photograph of the Hartmann whistle set-up kept in an anechoic chamber

2.2 Hartmann whistle geometry

Table 1 – The Hartmann cavity geometry and other dimensions

NPR	Separation (S), mm	Length (L), mm	Diameter (D), mm
3.0	16	45	11
5.0	32	45	11

Table 1 gives the details of Hartmann cavity geometry. It also gives the separation (S) between the jet orifice and the mouth of the cavity. The mouth of the cavity is kept at the end of the second shock cell of the under-expanded jet. As the NPR increases the shock cell length increases, which in turn results in increased separation. It is important to place the mouth of the Hartmann cavity at these specified locations in order for it to operate. These locations are often termed as regions of instability in literature (1)

2.3 Instrumentation

Far-field acoustic pressure is measured using a 1/4-inch pre-polarized microphone (PCB Model 378C01). The sensitivity of the microphone is 2 mV/Pa at 250 Hz. A piezoelectric sensor (PCB Model 113B27) is used to measure the gas oscillation pressure at the closed end of the cavity. The far-field acoustic and gas oscillation signals are acquired at a sampling rate of 250 kS/sec. The microphone has a flat response in the frequency range of 4 Hz to 70 kHz, within 1 dB variation. A pistonphone (B&K Type 4228) is used to calibrate the microphone, at 250 Hz and 124 dB. The data acquired is low-pass filtered at 70 kHz using an analog filter (Krohn-Hite Model 3364) to avoid aliasing. A 16-bit resolution, 8-channel data acquisition board (National Instruments PCI-6143) is used to acquire the data. Measurements of pressure inside the settling chamber is monitored by a Bourdon gauge. The reference pressure used to calculate SPL and OASPL is 20 μPa. The uncertainty in SPL calculations is within ±1 dB. The microphone angle measured, has an uncertainty of ±1° in the directivity experiments. The error in axial static pressure measurement probe location is ±0.1 mm. Schlieren flow visualization technique was used to study the shock dynamics. High speed Schlieren images were captured using Phantom v1212 high speed camera at the frame rate of 40,000 Hz.

3 RESULTS AND DISCUSSION

3.1 Schlieren Flow Visualization Data

Figure 3 shows a Schlieren image encapsulating all the flow features of the Hartmann whistle phenomenon. It shows the under-expanded jet emanating from the orifice impinging the mouth of the Hartmann cavity axially. The complicated flow interaction of jet with the mouth of the cavity can also be seen. Also, since the mouth is place in the expansion region of the under-expanded jet we can see a stand-off shock upstream of the Hartmann cavity mouth. The oscillation of this stand-off shock is

responsible for the intense sound produced by this device. High speed images capture this shock dynamics more clearly.

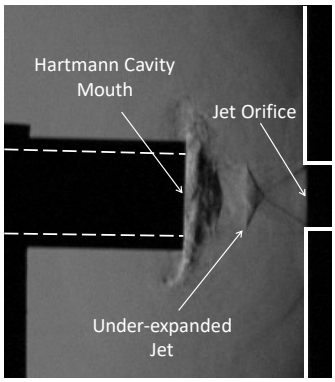

Figure 3 – The Schlieren image showing the complicated flow aspects involved in the operation of Hartmann cavity

3.1.1 NPR 3.0

Figure 4 (a) and (b) shows the high speed image sequences for the compression and expansion cycle, respectively. Compression cycle here is indicated by the movement of the stand-off shock towards the mouth of the Hartmann cavity (downstream direction). On the other hand, the expansion cycle is indicated by the movement of the stand-off shock away from the mouth of the Hartmann cavity (upstream direction). The inset number on each image refers to the frame number in the image sequence. Frames 244 and 258 represent the starting and ending of the compression cycle. Each successive frame is separated by 25 µsec, hence the time taken for compression cycle is 350 µsec. Frames 259 and 269 represent the starting and ending of the expansion cycle. These frames are separated by 250 µsec. It can be clearly seen that the compression cycle takes more time than the expansion cycle. This is due to the non-sinusoidal static pressure variation in an under-expanded jet. One full cycle takes around 600 µsec to complete which corresponds to a frequency value of 1.666 Hz. An interesting thing to note here is, the stand-off shock merges with the 1st shock cell when it moves in the upstream direction.

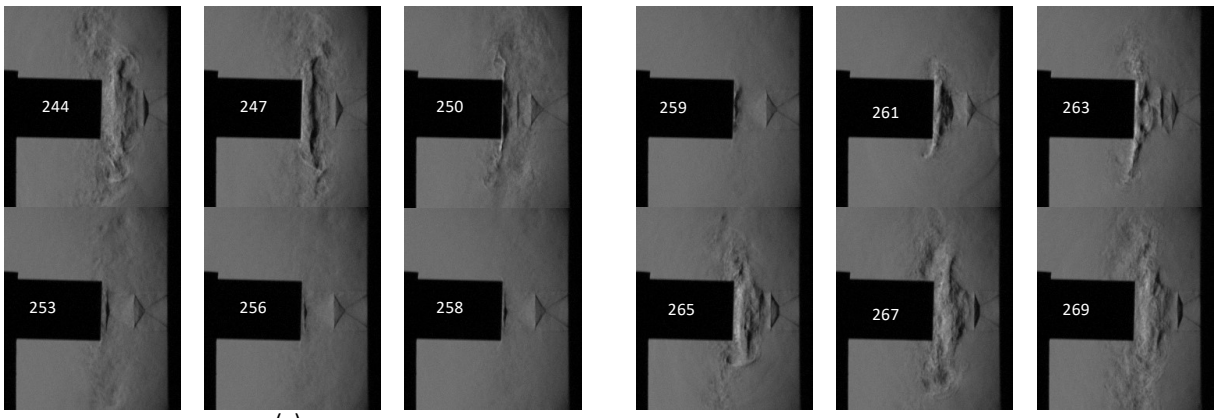

Figure 4 – High speed Schlieren sequence images for NPR = 3.0 (a) compression and (b) expansion cycles

3.1.2 NPR 5.0

Figure 5 (a) and (b) shows the high speed image sequences for the compression and expansion cycle, respectively. The inset number on each image refers to the frame number in the image sequence. Frames 87 and 104 represent the starting and ending of the compression cycle. Each frame is separated by 25 µsec, hence the time taken for compression cycle is 425 µsec. Frames 105 and 115 represent the starting and ending of the expansion cycle. These frames are separated by 250 µsec. It can be clearly seen that the compression cycle takes more time than the expansion cycle. This again is due to the non-sinusoidal static pressure variation in an under-expanded jet. One full cycle takes around 600 µsec to complete which corresponds to a frequency value of 1.481 kHz. Unlike NPR 3.0 case, here the stand-off shock does not merge with the 1st shock cell when it moves in the upstream direction.

Another, interesting observation is that the expansion cycle takes the same amount of time, whereas the compression cycle in NPR 5.0 case takes longer time than NPR 3.0 case.

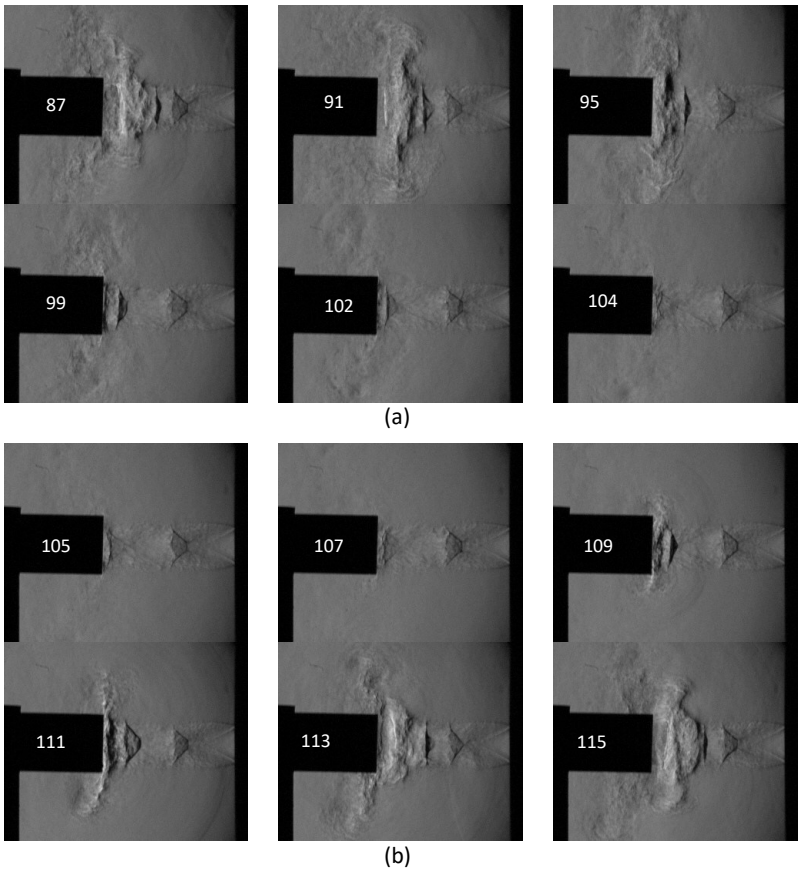

Figure 5 – High speed Schlieren sequence images for NPR = 5.0 (a) compression and (b) expansion cycles

3.2 Sound Pressure Level (SPL)

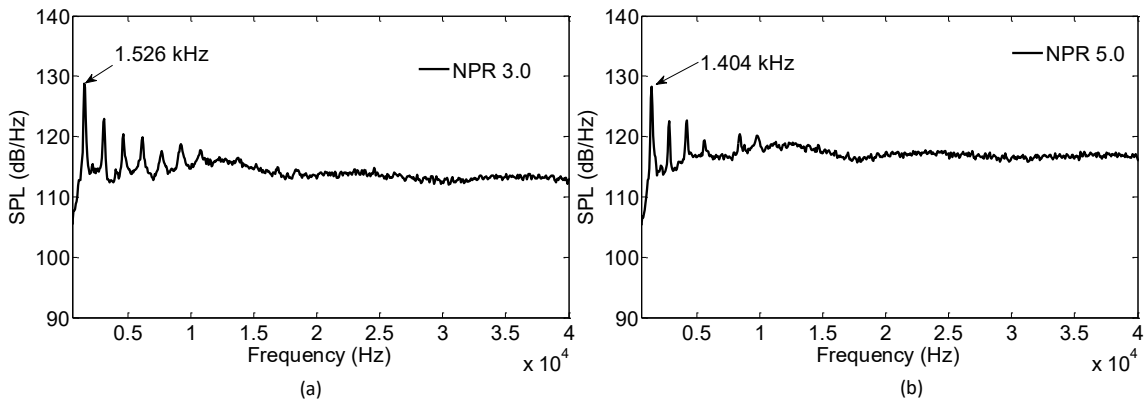

Figure 6 – Sound Pressure Level (a) NPR = 3.0 and (b) NPR = 5.0

SPL is measured at distance 40 times the jet orifice diameter (R=400 mm). These measurements can be safely assumed to be in the far-field where plane wave assumption is valid. Figure 6 (a) and (b) shows the SPL measured at 90 deg and 400 mm from the orifice center, at two different NPRs 3.0 and 5.0, respectively. The Hartmann whistle clearly shows distinct peaks in the spectrum. The fundamental mode frequency corresponds to 1.526 Hz and 1.404 kHz respectively. The frequency obtained is closer to the quarter-wave-tube frequency. When compared to NPR 3.0 case, the frequency of oscillation is lesser for NPR 5.0, which is also corroborated by the frequency data obtained from high speed Schlieren images.

3.3 Overall Sound Pressure Level (OASPL): Directivity

Figure 7 (a) and (b) shows the directivity (OASPL) at different emission angles at NPR = 3 and 5, respectively. We can see that there is very little change in directivity at different emission angles. The OASPL data is not available for angles below 40° and above 120° at a radius of 400 mm. Below 40° the jet will impinge on the microphone which can damage the sensor, whereas beyond 120° the sensor is in the shadow of orifice, hence measurements were limited between 40 deg-120 deg. It can be clearly seen that the maximum directivity occurs around 40 deg, which is in the downstream direction. This observation is consistent with early findings (11).

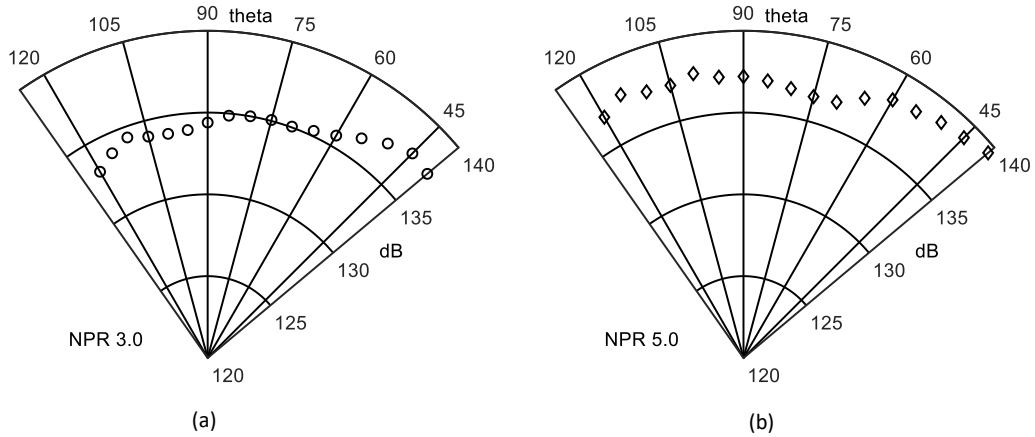

Figure 7 – Directivity (a) NPR = 3.0 and (b) NPR = 5.0

3.4 Cavity Gas Oscillations

The pressure at the closed end of the Hartmann cavity was measured. The closed end pressure would mimic the gas oscillation inside the cavity. Figure 8 shows the gas oscillation pressure at the closed end of the cavity at NPRs 3.0 and 5.0, respectively. For NPR 3.0, expansion cycle takes around 380 µsec and compression cycle takes around 240 µsec. For NPR 5.0, expansion cycle takes around 432 µsec and compression cycle takes around 288 µsec. For both the NPRs the expansion cycle takes more time than compression cycle. This is due to the non-symmetry in the static pressure variation in under-expanded jets. The time taken for compression and expansion cycle matches well with that found using high speed Schlieren data, for both the NPRs.

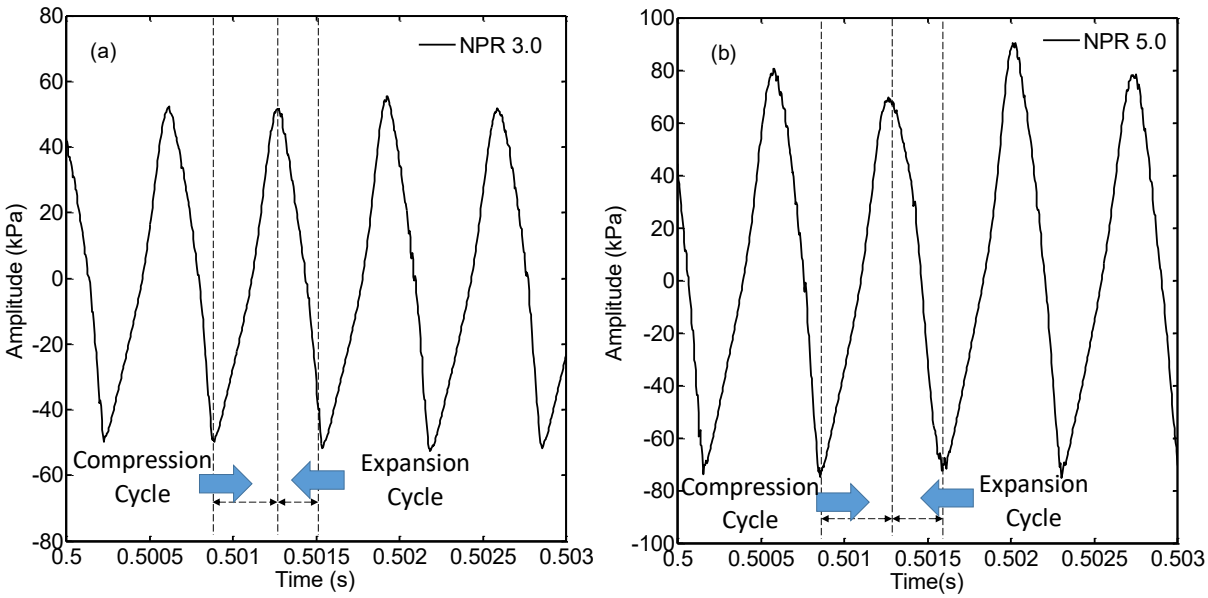

Figure 8 – Gas oscillations inside the cavity (closed end) (a) NPR = 3.0 and (b) NPR = 5.0

4 CONCLUSIONS

Experimental study was conducted on a cylindrical Hartmann whistle to understand the shock dynamics associated with it. The aero-acoustic performance is measured in terms of SPL and OASPL, at two different NPRs. Intense sound field of the order of 130 dB is produced at both NPRs. Maximum directivity occurs at 40 deg. It was found that, the resonance frequency at NPR 5.0 is less than that at NPR 3.0. All the data from high speed Schlieren, the microphone and the piezoelectric sensor at the closed end, matched very well.

The aero-acoustic data presented n this study is mixed with the jet noise data. Hence, it is difficult to comment on the resonance quality based on the aero-acoustic data alone. In the present study, the flow imping on the cavity is just little above sonic. Since, some of the applications of this cavity can be found in hypersonic vehicle fore-body, it would be interesting to do similar studies at high supersonic Mach numbers. Also, it would be interesting to study Hartmann cavities with different internal profiles.

ACKNOWLEDGEMENTS

We are grateful to Prof. Baburaj A. P, for lending us the high speed camera used in this study, which was funded by the grant Sr/FST/ ETII-064/2015 from DST, Government of India.

REFERENCES

1. Smith T, Powell A. Experiments concerning the hartmann whistle. University of California; 1964.
2. Smith T, Powell A. On the Mechanism of the Hartmann Whistle. J Acoust Soc Am. 1964;36(5):1018.
3. Raman G, Kibens V. Active Flow Control Using Integrated Powered Resonance Tube Actuators. In: 31st AIAA Fluid Dynamics Conference & Exhibit. Anaheim, CA; 2001. p. 3024.
4. Raman G, Srinivasan K. The powered resonance tube: From Hartmann's discovery to current active flow control applications. Prog Aerosp Sci [Internet]. 2009;45:97–123.
5. Raman G, Khanafseh S, Cain AB, Kerschen E. Development of high bandwidth powered resonance tube actuators with feedback control. J Sound Vib. 2004;269(3–5):1031–62.
6. Sarohia V, Back LH. Experimental investigation of flow and heating in a resonance tube. J Fluid Mech. 1979;94:1979.
7. Raman G, Kibens V, Cain A. Advanced actuator concepts for active aeroacoustic control. In: 6th AIAA/CEAS Aeroacoustics Conference. Lahaina, Hawaii; 2000.
8. Sreejith GJ, Narayanan S, Jothi TJS, Srinivasan K. Studies on conical and cylindrical resonators. Appl Acoust. 2008;69(12):1161–75.
9. Narayanan S, Srinivasan K, Sundararajan T. Aero-acoustic features of internal and external chamfered Hartmann whistles: A comparative study. J Sound Vib. 2014;333(3):774–87.
10. Narayanan S, Srinivasan K, Sundararajan T, Ramamurthi K. Acoustic characteristics of chamfered Hartmann whistles. J Sound Vib. 2011;330(11):2470–96.
11. Narayanan S, Bhave P, Srinivasan K, Ramamurthi K, Sundararajan T. Spectra and directivity of a Hartmann whistle. J Sound Vib. 2009;321(3–5):875–92.
12. Narayanan S, Srinivasan K, Sundararajan T. Effect of lip thickness on the aero-acoustic features of Hartmann whistle. Proc Inst Mech Eng Part G J Aerosp Eng. 2013;228(8):1302–13.
13. Narayanan S, Srinivasan K, Sundararajan T. Acoustic characteristics of external chamfered Hartmann whistles. Appl Acoust. 2013;74(9):1104–16.
14. Narayanan S, Srinivasan K, Sundararajan T. Atomization in the acoustic field of a Hartmann whistle. Int

J Spray Combust Dyn. 2013;5(1):1–24.

15. Lu H, Liu W. Investigation of thermal protection system by forward-facing cavity and opposing jet combinatorial configuration. Chinese J Aeronaut. 2013;26(2):287–93.

16. Huang W, Yan L, Liu J, Jin L, Tan JG. Drag and heat reduction mechanism in the combinational opposing jet and acoustic cavity concept for hypersonic vehicles. Aerosp Sci Technol. 2015;42:407–14.

17. Li X, Hu Z, Jiang Z. Numerical investigation on the thermal protection mechanism for blunt body with forward-facing cavity. Sci China Technol Sci. 2016;59(7):1120–9.